JACS
JOURNAL OF THE AMERICAN CHEMICAL SOCIETY

Communication

pubs.acs.org/JACS

Metallic WO_2–Carbon Mesoporous Nanowires as Highly Efficient Electrocatalysts for Hydrogen Evolution Reaction

Rui Wu,[†,‡] Jingfang Zhang,[†] Yanmei Shi,[†] Dali Liu,[†] and Bin Zhang*[,†]

[†]Department of Chemistry, School of Science, Tianjin University, and Collaborative Innovation Center of Chemical Science and Engineering, Tianjin 300072, P.R. China

[‡]School of Chemical Engineering and Technology, Tianjin University, Tianjin 300072, P.R. China

Supporting Information

ABSTRACT: The development of electrocatalysts to generate hydrogen, with good activity and stability, is a great challenge in the fields of chemistry and energy. Here we demonstrate a "hitting three birds with one stone" method to synthesize less toxic metallic WO_2–carbon mesoporous nanowires with high concentration of oxygen vacancies (OVs) via calcination of inorganic/organic WO_3–ethylenediamine hybrid precursors. The products exhibit excellent performance for H_2 generation: the onset overpotential is only 35 mV, the required overpotentials for 10 and 20 mA/cm^2 are 58 and 78 mV, the Tafel slope is 46 mV/decade, the exchange current density is 0.64 mA/cm^2, and the stability is over 10 h. Further studies, in combination with density functional theory, demonstrate that the unusual electronic structure and the large amount of active sites, generated by the high concentration of OVs, as well as the closely attached carbon materials, were key factors for excellent performance. Our results experimentally and theoretically establish metallic transition metal oxides (TMOs) as intriguing novel electrocatalysts for H_2 generation. Such TMOs with OVs might be promising candidates for other energy storage and conversion applications.

The depletion of fossil fuels and severe environmental problems have garnered much attention for clean and sustainable energy sources.[1] Hydrogen is a good candidate because it is efficient, clean, and sustainable. Hydrogen evolution reaction (HER) from electrocatalytic water splitting is a promising method to produce H_2,[2] but the best HER catalysts—platinum and Pt-based materials[3]—are expensive and scarce. Since the first report of the use of MoS_2 nanoparticles for HER,[4] the search for inexpensive and earth-abundant electrocatalysts to replace Pt for HER has undergone rapid development.[5] However, most of the materials considered are semiconductors, having poor conductivity and anisotropic electron transfer that hinder their further development.[6] Generally, two strategies have been adopted to enhance their conductivity: synthesizing metallic electrocatalysts (such as transition metal sulfides and selenides)[7] or using substrates with high electric conductivity (e.g., carbon materials and noble metals).[7f,8] Both can improve HER performance, but the complicated process and/or poisonous components[7d,f,8] during the synthesis make them insufficient to replace Pt.

An alternative is to search for novel highly efficient HER electrocatalysts. Transition metal oxides (TMOs), which have recently found potential applications in oxygen evolution reaction,[9] oxygen reduction reaction,[9] and photochemical reduction,[10] are of great interest because of their stability, abundance, easy accessibility, and environmental friendliness. The opportunity to effectively generate and take advantage of oxygen vacancies (OVs) in TMOs is of particular importance.[10,11] OVs have been reported to enhance catalytic activities by narrowing the band gaps and providing active sites.[11b] As a result, some TMOs with high concentrations of OVs are metallic and possess many active catalytic sites, making them excellent candidates for electrocatalysis. However, to date, the use of these metallic TMOs, supported on highly conductive substrates for HER, especially with porous structure which can provide larger specific area and more active sites,[12] has been a big challenge.

Here we demonstrate a novel "oxygen extraction" approach to synthesize less toxic metallic WO_2–carbon mesoporous nanowires (MWCMNs) with high concentration of OVs via one-pot calcination of WO_3–EDA (EDA = ethylenediamine) inorganic/organic hybrids (Figure 1; see Supporting Information (SI) for details). The facile "hitting three birds with one stone" strategy can endow the products with three characteristics: (1) mesoporous structures, (2) the *in situ*-formed carbon as rigid

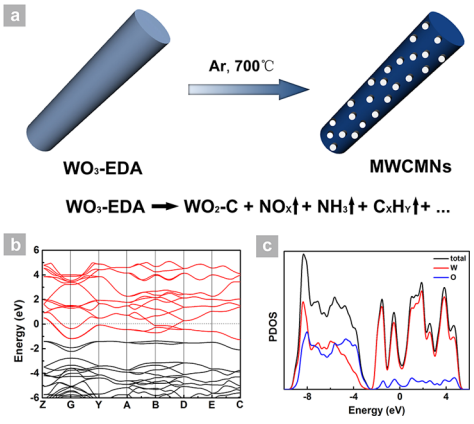

Figure 1. Synthetic schematic diagram (a), simulated band structure (b), and projected density of states (c) of metallic WO_2–carbon mesoporous nanowires (MWCMNs).

Received: February 6, 2015
Published: May 20, 2015

DOI: 10.1021/jacs.5b01330
J. Am. Chem. Soc. 2015, 137, 6983–6986

substrate and electron mobility promoter, and (3) the presence of a large amount of OVs in WO_2 making them metallic. The as-prepared MWCMNs show outstanding HER performance. Experimental and theoretical data reveal that the unusual electronic structure and greater number of active sites, generated by the high concentration of OVs, as well as the closely attached carbon, are key factors for excellent performance.

WO_3–EDA inorganic/organic hybrid precursors were synthesized via a reported procedure.[13] Scanning electron microscopy (SEM, Figure 2a) and transmission electron microscopy (TEM, Figure 2b) images indicated the synthesis of nanowire-like WO_3–EDA. Figure S2 reveals that only W^{6+} appears in the products. The X-ray diffraction (XRD) pattern, Fourier transform infrared and UV/vis spectra, and thermogravimetric analysis (Figures S3–S6) suggested successful synthesis of inorganic/organic WO_3–EDA nanowires.

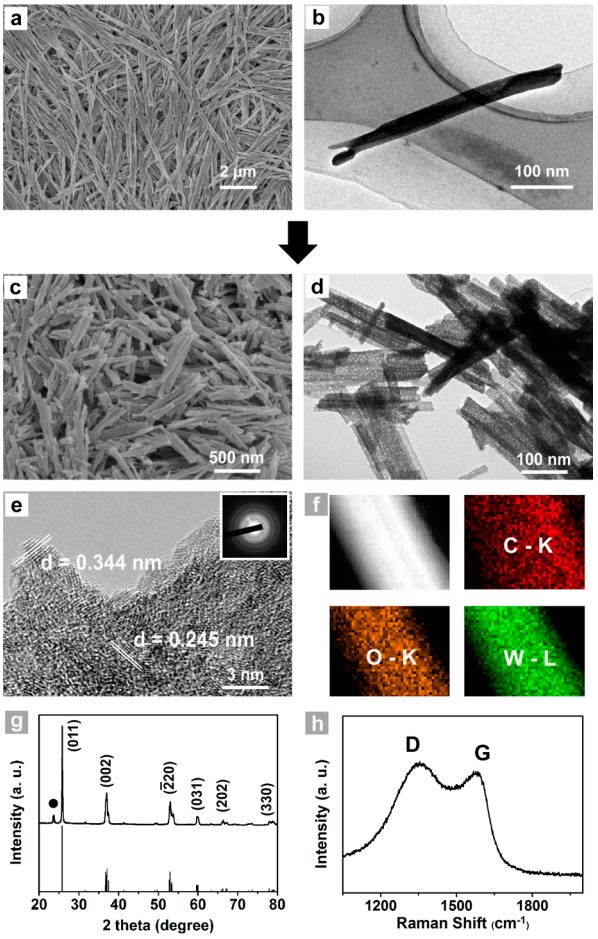

Figure 2. (a) SEM and (b) TEM images of WO_3–EDA inorganic/organic precursors. (c) SEM, (d) TEM, (e) HRTEM and the associated SAED pattern (inset), and (f) STEM–EDS mapping images of C, O, and W of MWCMNs. (g) XRD pattern of MWCMNs (black dot indicates carbon species; the other peaks are ascribed to monoclinic WO_2 (PDF No. 32-1393), with its standard pattern given at the bottom). (h) Raman spectrum of MWCMNs.

When calcinated in Ar gas flow at 700 °C for 5 h, these WO_3–EDA inorganic/organic hybrids were transformed into MWCMNs. SEM (Figure 2c) revealed that the products were synthesized with retention of 1D structure, and TEM (Figure 2d) revealed the generation of mesoporous structure, as demonstrated by the evident contrast as well as Brunauer–Emmett–Teller analysis (Figure S10). Moreover, high-resolution (HR) TEM (Figure 2e) and the associated SAED pattern (Figure 2e inset) showed that the products were polycrystalline. The lattice fringes in Figure 2e, with measured interplanar spacings of 0.344 and 0.245 nm, corresponded to (011) and (002) planes of monoclinic WO_2, respectively. Figure 2f shows the scanning transmission electron microscopy (STEM)–energy-dispersive X-ray spectroscopy (EDS) mapping images of a single nanowire, confirming the existence and uniform distribution of W, O, and C.

XRD and Raman spectroscopy were further used to confirm the phase and purity of products. XRD (Figure 2g) indicated that the as-prepared mesoporous nanowires consisted of monoclinic structured WO_2 with lattice parameters $a = 0.558$, $b = 0.490$, and $c = 0.556$ nm (PDF No. 32-1393), corresponding to the results of the HRTEM image in Figure 2e. The peak around 24° is ascribed to carbon species. No peaks of any other impurities were observed, indicating the high purity of products. Raman spectroscopy (Figure 2h) was performed to confirm the carbon species in as-prepared products. Two characteristic peaks for graphitized carbon structure at 1347 and 1583 cm^{-1}, the latter matching the value of pristine graphene (1586 cm^{-1}),[8c] revealed that carbon content in MWCMNs can be indexed to graphite. Such carbon materials not only serve as rigid substrates to prevent nanoparticles from agglomeration (Figure S12) but also benefit the fast electron transfer.[8c] These results confirm that MWCMNs were successfully generated via calcination of WO_3–EDA inorganic/organic hybrid precursors. WO_3 porous nanowires (WPNs) were also prepared, via calcination of WO_3–EDA hybrids in air with other conditions unchanged, for comparison (see SI for details, particularly Figures S14–S16).

The synthetic procedure is highlighted by its novel "oxygen extraction" concept. During the calcination of WO_3–EDA precursors, N-atoms in EDA could extract O-atoms in WO_3 to form NO_x, so that the tungsten oxides in products would be WO_2. We first detected the concentratiosn of NO and NO_2 during the transformation. As shown in Figure S7, NO and NO_2 were detected above 200 °C. Moreover, the components in off-gas were also detected to clarify the whole reaction mechanism (Figure S8). Besides NO_x, C_xH_y and NH_3 were also detected. Thus, the transformation from WO_3–EDA precursors into MWCMNs was confirmed, in which N-atoms in EDA extracted O-atoms in WO_3 to form NO_x, while other atoms in EDA transformed into NH_3 and C_xH_y. Also, some C-atoms were converted to *in situ*-formed carbon (Figure 1a). It should be noted that the whole transformation was much more complicated, and we give only a reasonable simplified model.

Previous studies showed that the different valences of W between $W_{18}O_{49}$ and WO_3 can explain the OVs in $W_{18}O_{49}$.[10] Here we performed X-ray photoelectron spectroscopy to confirm the chemical states of W in MWCMNs and WPNs, testifying to the presence of OVs in as-prepared MWCMNs. Peaks of MWCMNs in the W 4f region (Figure S17a) revealed the existence of not only W^{4+} (32.40 eV) for WO_2, but also W^{5+} (33.90 eV) and W^{6+} (35.52 and 37.68 eV) due to the strong surface oxidation in the air. In contrast, peaks of WPNs in the W 4f region (Figure S17b) could only be assigned to W^{6+} (35.34 and 37.56 eV). The different W valences between MWCMNs and WPNs clearly demonstrate the presence of a large number of OVs in MWCMNs. What's more, OVs in tungsten oxides were also demonstrated by their strong vis/NIR absorption and blue emission band due to the excitation of conduction band electrons, which can be ascribed to the localized surface plasmon

DOI: 10.1021/jacs.5b01330
J. Am. Chem. Soc. 2015, 137, 6983–6986

resonances.[10,11] Compared with WPNs, MWCMNs showed unusual photophysical properties, as indicated by UV/vis spectra (Figure S18). The big absorption tail in the range of 490−800 nm provided strong evidence that MWCMNs had a large amount of OVs. A strong blue emission band at ∼440 nm was observed in the photoluminescence spectrum (Figure S19), further indicating the high concentration of OVs in MWCMNs.

To examine their electrocatalytic HER activity, MWCMNs were loaded onto glassy carbon (GC) electrode (the loading amount was ∼0.35 mg cm^{-2}, and all tests were carried out in 0.5 M H_2-saturated H_2SO_4). For comparison, bare GC, WPNs, and commercially available 20 wt% Pt/C (Johnson Matthey) were also tested with same deposition amount. Figure 3a shows the

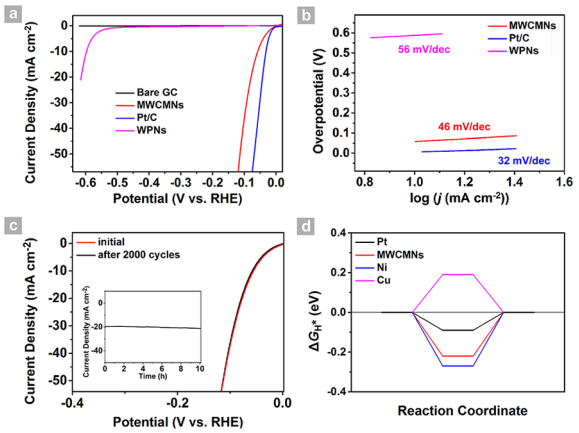

Figure 3. (a) Polarization curves of bare GC, MWCMNs, WPNs, and Pt/C. (b) Tafel plots of MWCMNs, Pt/C, and WPNs (*I*−*R* corrected, see Figure S20 for initial curves). (c) Polarization curves of MWCMNs initially and after 2000 CV scans. . Inset in (c) is time-dependent current density curve for MWCMNs under static overpotential of 58 mV for 10 h. (d) HER free energy diagram calculated at the equilibrium potential for MWCMNs and some other metal electrocatalysts.

polarization curves after *I*−*R* correction (see Figure S20 for initial curves). Pt/C unquestionably exhibited the highest performance, with an onset overpotential of nearly zero, and bare GC exhibited negligible HER activity. Surprisingly, as-prepared MWCMNs exhibited an onset overpotential of only 35 mV, and the current rose sharply under more negative potentials, revealing they were highly active electrocatalysts for HER. Overpotentials of 58 and 78 mV can lead to current densities of 10 and 20 mA/cm^2, respectively. These values of the as-prepared MWCMNs were better than those of many other reported HER electrocatalysts based on non-noble-metal materials, especially metallic transition metal dichalcogenides (EM_2; E = Fe, Co, Ni, Mo, W, M = S, Se) (Table S1). Additionally, as shown by electrochemical impedance spectroscopy (Figures S21−S23), the sharply decreased diameter of MWCMNs demonstrated improved HER kinetics. For electrocatalysts, the electron states near the Fermi level are the key factors for their activity.[7e] As shown in Figure 1c, the Fermi level crossed the conduction band of MWCMNs. The unique electron structure near the Fermi level is associated with the narrowed band gap caused by the large concentration of OVs. Also, the closely attached carbon substrates could contribute to HER activity, as they can lead to fast electron transfer.

As shown in Figure 3b, Tafel slope for commercial Pt/C was ∼32 mV/decade, corresponding to literature values. For MWCMNs, the Tafel slope was calculated to be 46 mV/decade, revealing an excellent HER activity with Volmer−Heyrovsky mechanism. This value was among the best ones for electrocatalysts composed of metallic EM_2 (Table S1). The exchange current density i_0 (calculated by extrapolation using the Tafel plot)[7f] was determined to be 0.64 mA/cm^2. This was the largest value for all non-noble-metal HER electrocatalysts (Table S1), revealing the large electrochemically active surface area. Such superior electrocatalytic HER performance can be explained as follows: (1) the high concentration of OVs played a vital role, as they could narrow the band gap and provide more active sites for MWCMNs; (2) the unique mesoporous structure composed of highly crystalline nanoparticles led to the exposure of many more active sites and the effective movement of electrons and reacting agents; and (3) carbon would promote electron transfer and act as a rigid substrate, which could improve the stability and resistance toward oxidation.

We further probed the stability of as-prepared MWCMNs by a long-term cycling test. The polarization curves measured before and after 2000 cycles were compared. The final polarization curve exhibit nearly no difference from the initial one (Figure 3c). Inset in Figure 3c demonstrates that the HER performance remained nearly unchanged for more than 10 h. These stable measurements (Figures S25 and S26) show that the as-prepared MWCMNs are highly stable electrocatalysts for HER.

Finally, density functional theory (DFT) was applied to calculate the position of valence and conduction bands from the band structure and the projected density of states (PDOS), as well as the HER Gibbs free energy, which can give strong theoretical proof and a direct explanation for the superior HER performance. Contrary to semiconductor WO_3,[14] as the Dirac cone downshifts, MWCMNs show no clear band gap (Figure 1b). The PDOS of MWCMNs also shows that the valence and conduction bands sharply downshift. Thus, the conduction band of MWCMNs is crossed by the Fermi level, making them metallic and suggesting an enhanced electron mobility; thus, they are promising electrocatalysts (Figure 1c). For most electrocatalysts, the whole HER approach consists of three steps: (1) $H^+ + e^-$, (2) catalyst−H*, and (3) H_2 products.[15] The optimal Gibbs free energy of catalyst−H* (ΔG_{H^*}) is 0, as first reported by Parsons.[16] If the value is too large, it will be difficult to absorb H* at the catalysts, while if the value is too small, the absorbed H* will hardly desorb to generate H_2, instead occupying the active sites and poisoning the HER process. So, it is reasonable to use the value of $|\Delta G_{H^*}|$ to describe the HER performance of various electrocatalysts. The $|\Delta G_{H^*}|$ value of the most efficient catalyst, Pt, is nearly 0.09 eV, which is very close to thermoneutral.[15] We calculated the $|\Delta G_{H^*}|$ value of MWCMNs to be 0.22 eV (Figure 3d), comparable to those of non-noble-metal catalysts (Table S2). The experimental value of i_0 and the theoretical value of ΔG_{H^*} are shown on the volcano curve (Figure S28). The performance of each electrocatalyst could be quantitatively measured from its position on the volcano curve (the electrocatalyst is good if its position is close to the peak). The HER activities of MWCMNs determined by both i_0 and ΔG_{H^*} (red square in Figure S28) are better than those of non-noble-metal and metal-free electrocatalysts and comparable to those of some well-known highly efficient noble-metal electrocatalysts, such as Pt and Pd. Also, we calculated i_0 from the true surface (see SI for details) and marked the position determined in this way (blue square in Figure S28); it is comparable to that of MoS_2. Thus, as-prepared MWCMNs have been experimentally and theoretically proved to be highly efficient HER electrocatalysts. It should be noted that our DFT calculations do not

DOI: 10.1021/jacs.5b01330
J. Am. Chem. Soc. 2015, 137, 6983−6986

take into consideration all the experimental details. We optimize MWCMNs to ideal monoclinic WO_2, ignoring the effect of carbon. Thus, our DFT results are only a guide, despite their good agreement with our experimental results. On the other hand, carbon materials have been widely used to enhance electrochemical activity,[8c] so the optimization in our work is justified.

In summary, less toxic MWCMNs with high concentrations of OVs have been successfully synthesized via a novel "oxygen extraction" treatment of inorganic/organic WO_3−EDA hybrids. This handy "hitting three birds with one stone" strategy endows the products with three characteristics: mesopores, *in situ*-formed carbon, and metallic WO_2 with rich OVs. The as-prepared MWCMNs show outstanding performance in HER. The onset overpotential is only 35 mV, the Tafel slope is calculated to be 46 mV/decade, and the high activity can be maintained for more than 10 h. Moreover, the current densities of 10 and 20 mA/cm^2 require overpotentials of 58 and 78 mV, respectively. Experimental and theoretical data reveal that the unusual electron state near the Fermi level and the much higher number of active sites caused by the high concentration of OVs, as well as the closely attached carbon, are key factors. This particular material describes a novel route to cheap and easily accessible metallic TMO materials with superior HER performance and other promising energy storage and conversion applications.

■ ASSOCIATED CONTENT

Supporting Information

Details of synthesis, characterization, and theoretical calculations; Figures S1−S28; and Tables S1 and S2. The Supporting Information is available free of charge on the ACS Publications website at DOI: 10.1021/jacs.5b01330.

■ AUTHOR INFORMATION

Corresponding Author

*bzhang@tju.edu.cn

Notes

The authors declare no competing financial interest.

■ ACKNOWLEDGMENTS

We appreciate the discussions and help from Prof. Helmuth Möhwald and Prof. Xingang Li, and acknowledge financial support from NSFC (No. 21422104).

■ REFERENCES

(1) (a) Dresselhaus, M. S.; Thomas, I. L. *Nature* **2001**, *414*, 332. (b) Turner, J. A. *Science* **2004**, *305*, 972.

(2) (a) Cook, T. R.; Dogutan, D. K.; Reece, S. Y.; Surendranath, Y.; Teets, T. S.; Nocera, D. G. *Chem. Rev.* **2010**, *110*, 6474. (b) Hochbaum, A. I.; Yang, P. *Chem. Rev.* **2012**, *110*, 527.

(3) Stamenkovic, V. R.; Mun, B. S.; Arenz, M.; Mayrhofer, K. J.; Lucas, C. A.; Wang, G.; Ross, P. N.; Markovic, N. M. *Nat. Mater.* **2007**, *6*, 241.

(4) Hinnemann, B.; Moses, P. G.; Bonde, J.; Jørgensen, K. P.; Nielsen, J. H.; Horch, S.; Chorkendorff, I.; Nørskov, J. K. *J. Am. Chem. Soc.* **2005**, *127*, 5308.

(5) (a) Zheng, Y.; Jiao, Y.; Jaroniec, M.; Qiao, S. Z. *Angew. Chem., Int. Ed.* **2015**, *54*, 2. (b) Faber, M. S.; Jin, S. *Energy Environ. Sci.* **2014**, *7*, 3519. (c) Wan, C.; Regmi, Y. N.; Leonard, B. M. *Angew. Chem., Int. Ed.* **2014**, *53*, 6407. (d) Tian, J. Q.; Liu, Q.; Asiri, A. M.; Sun, X. P. *J. Am. Chem. Soc.* **2014**, *136*, 7587. (e) Liao, L.; Wang, S.; Xiao, J.; Bian, X.; Zhang, Y.; Scanlon, M. D.; Hu, X.; Tang, Y.; Liu, B.; Girault, H. H. *Energy Environ. Sci.* **2014**, *7*, 387. (f) Kibsgaard, J.; Jaramillo, T. F. *Angew. Chem., Int. Ed.* **2014**, *53*, 14433. (g) Jiang, P.; Liu, Q.; Liang, Y. H.; Tian, J. Q.; Asiri, A. M.; Sun, X. P. *Angew. Chem., Int. Ed.* **2014**, *53*, 12855. (h) Gong, M.; Zhou, W.; Tsai, M. C.; Zhou, J. G.; Guan, M. Y.; Lin, M. C.; Zhang, B.; Hu, Y. F.; Wang, D. Y.; Yang, J.; Pennycook, S. J.; Hwang, B. J.; Dai, H. J. *Nat. Commun.* **2014**, *5*, 4695. (i) Xu, Y. F.; Gao, M. R.; Zheng, Y. R.; Jiang, J.; Yu, S. H. *Angew. Chem., Int. Ed.* **2013**, *52*, 8546. (j) Xu, Y.; Wu, R.; Zhang, J. F.; Shi, Y. M.; Zhang, B. *Chem. Commun.* **2013**, *49*, 6656. (k) Sun, Y.; Liu, C.; Grauer, D. C.; Yano, J.; Long, J. R.; Yang, P.; Chang, C. J. *J. Am. Chem. Soc.* **2013**, *135*, 17699. (l) Popczun, E. J.; McKone, J. R.; Read, C. G.; Biacchi, A. J.; Wiltrout, A. M.; Lewis, N. S.; Schaak, R. E. *J. Am. Chem. Soc.* **2013**, *135*, 9267. (m) Esposito, D. V.; Hunt, S. T.; Stottlemyer, A. L.; Dobson, K. D.; McCandless, B. E.; Birkmire, R. W.; Chen, J. G. *Angew. Chem., Int. Ed.* **2010**, *49*, 9859. (n) Le Goff, A.; Artero, V.; Jousselme, B.; Tran, P. D.; Guillet, N.; Metaye, R.; Fihri, A.; Palacin, S.; Fontecave, M. *Science* **2009**, *326*, 1384. (o) Chen, W. F.; Sasaki, K.; Ma, C.; Frenkel, A. I.; Marinkovic, N.; Muckerman, J. T.; Zhu, Y.; Adzic, R. R. *Angew. Chem., Int. Ed.* **2012**, *51*, 6131.

(6) (a) Kibsgaard, J.; Chen, Z.; Reinecke, B. N.; Jaramillo, T. F. *Nat. Mater.* **2012**, *11*, 963. (b) Merki, D.; Hu, X. *Energy Environ. Sci.* **2011**, *4*, 3878. (c) Jaramillo, T. F.; Jorgensen, K. P.; Bonde, J.; Nielsen, J. H.; Horch, S.; Chorkendorff, I. *Science* **2007**, *317*, 100. (d) Karunadasa, H. I.; Montalvo, E.; Sun, Y.; Majda, M.; Long, J. R.; Chang, C. J. *Science* **2012**, *335*, 698. (e) Cheng, L.; Huang, W. J.; Gong, Q. G.; Liu, C. H.; Liu, Z.; Li, Y. G.; Dai, H. J. *Angew. Chem., Int. Ed.* **2014**, *53*, 7860. (f) Vrubel, H.; Merki, D.; Hu, X. *Energy Environ. Sci.* **2012**, *5*, 6136.

(7) (a) Lukowski, M. A.; Daniel, A. S.; English, C. R.; Meng, F.; Forticaux, A.; Hamers, R. J.; Jin, S. *Energy Environ. Sci.* **2014**, *7*, 2608. (b) Voiry, D.; Yamaguchi, H.; Li, J.; Silva, R.; Alves, D. C. B.; Fujita, T.; Chen, M.; Asefa, T.; Shenoy, V. B.; Eda, G.; Chhowalla, M. *Nat. Mater.* **2013**, *12*, 850. (c) Faber, M. S.; Dziedzic, R.; Lukowski, M. A.; Kaiser, N. S.; Ding, Q.; Jin, S. *J. Am. Chem. Soc.* **2014**, *136*, 10053. (d) Lukowski, M. A.; Daniel, A. S.; Meng, F.; Forticaux, A.; Li, L.; Jin, S. *J. Am. Chem. Soc.* **2013**, *135*, 10274. (e) Kong, D.; Cha, J. J.; Wang, H.; Lee, H. R.; Cui, Y. *Energy Environ. Sci.* **2013**, *6*, 3553. (f) Kong, D.; Wang, H.; Lu, Z.; Cui, Y. *J. Am. Chem. Soc.* **2014**, *136*, 4897. (g) Zheng, Y.; Jiao, Y.; Zhu, Y.; Li, L. H.; Han, Y.; Chen, Y.; Du, A.; Jaroniec, M.; Qiao, S. Z. *Nat. Commun.* **2014**, *5*, 3783.

(8) (a) Zeng, Z.; Tan, C.; Huang, X.; Bao, S.; Zhang, H. *Energy Environ. Sci.* **2014**, *7*, 797. (b) Ge, X.; Chen, L.; Zhang, L.; Wen, Y.; Hirata, A.; Chen, M. *Adv. Mater.* **2014**, *26*, 3100. (c) Li, Y. G.; Wang, H. L.; Xie, L. M.; Liang, Y. Y.; Hong, G. S.; Dai, H. J. *J. Am. Chem. Soc.* **2011**, *133*, 7296.

(9) Liang, Y. Y.; Li, Y. G.; Wang, H. L.; Zhou, J. G.; Wang, J.; Regier, T.; Dai, H. J. *Nat. Mater.* **2011**, *10*, 780.

(10) Xi, G.; Ouyang, S.; Li, P.; Ye, J.; Ma, Q.; Su, N.; Bai, H.; Wang, C. *Angew. Chem., Int. Ed.* **2012**, *51*, 2395.

(11) (a) Manthiram, K.; Alivisatos, A. P. *J. Am. Chem. Soc.* **2012**, *134*, 3995. (b) Lei, F.; Sun, Y.; Liu, K.; Gao, S.; Liang, L.; Pan, B.; Xie, Y. *J. Am. Chem. Soc.* **2014**, *136*, 6826.

(12) (a) Zhao, X.; Bu, X. H.; Zhai, Q. G.; Tran, H.; Feng, P. Y. *J. Am. Chem. Soc.* **2015**, *137*, 1396. (b) Yu, Y.; Zhang, J.; Wu, X.; Zhao, W.; Zhang, B. *Angew. Chem., Int. Ed.* **2012**, *51*, 897.

(13) Hu, X.; Ji, Q.; Hill, J. P.; Ariga, K. *CrystEngComm* **2011**, *13*, 2237.

(14) Huda, M. N.; Yan, Y.; Moon, C.-Y.; Wei, S.-H.; Al-Jassim, M. M. *Phys. Rev. B* **2008**, *77*, No. 195102.

(15) (a) Greeley, J.; Jaramillo, T. F.; Bonde, J.; Chorkendorff, I. B.; Norskov, J. K. *Nat. Mater.* **2006**, *5*, 909. (b) Nørskov, J. K.; Bligaard, T.; Rossmeisl, J.; Christensen, C. H. *Nat. Chem.* **2009**, *19*, 37.

(16) Parsons, R. *Trans. Faraday Soc.* **1957**, *54*, 1053.

DOI: 10.1021/jacs.5b01330
J. Am. Chem. Soc. 2015, 137, 6983−6986